# C60CF2 BASED ORGANIC FIELD-EFFECT

# TRANSISTORS WITH ENHANCED AIR-

# **STABILITY**

Raj Kishen Radha Krishnan<sup>1\*</sup>, Brian J. Reeves<sup>3</sup>, Steven H. Strauss<sup>3</sup>, Olga V. Boltalina<sup>3</sup>, Björn Lüssem<sup>1,2\*</sup>

<sup>1</sup>Department of Physics, Kent State University, Kent, OH 44240, USA

<sup>2</sup> Advanced Materials and Liquid Crystal Institute, Kent State University, Kent, OH 44242, USA

<sup>3</sup> Department of Chemistry, Colorado State University, Fort Collins, CO 80523, USA

\*Corresponding author: <u>rradhakr@kent.edu</u>; blussem@kent.edu

**Keywords**: n-type, air-stable, fullerene, moisture, traps, oxygen

**Abstract.** Fullerenes and their derivatives are among the most commonly used electron transport materials. However, the use of fullerenes is limited by their low stability in ambient air. Here, we test the hypothesis that the air-stability of fullerene-based electron transport materials can be improved by adding fluorinated functional groups, making the materials less susceptible to degradation by interaction with oxygen and moisture. As proof for the concept,  $C_{60}CF_2$  based Organic Field-Effect Transistors (OFETs) are studied. An average mobility of  $\mu = (0.83 \pm$ 

0.52)  $cm^2V^{-1}s^{-1}$  is found, with a maximum mobility of  $\mu = 2.02$   $cm^2V^{-1}s^{-1}$ . Compared to identical C<sub>60</sub> OFETs, C<sub>60</sub>CF<sub>2</sub> based OFETs degrade at a much lower rate and even sustain exposure times of up to 60 h in ambient air.

## **INTRODUCTION**

Over the last few years the performance of organic transistors has improved progressively making them viable candidates for a number of applications. Organic transistors could find applications in flexible displays,<sup>1</sup> data storage,<sup>2</sup> gas sensors,<sup>3</sup> smart cards,<sup>4</sup> low cost RFID tags<sup>5</sup> etc. However, there are a number of factors hindering the efficient use of OFETs in such applications, including low charge carrier mobility, large contact resistance,<sup>6</sup> poor reproducibility<sup>7</sup> and stability<sup>8,9</sup>. While significant progress has been made in improving the mobility with recent single crystal OFETs reporting mobility<sup>10</sup> values as high as  $16.4 \text{ cm}^2 V^{-1} \text{s}^{-1}$  and contact resistances as low as  $29 \Omega \text{cm}$ ,<sup>11</sup> the issue of stability still warrants further attention, especially for n-type semiconductors. In contrast to hole-transport materials, where a number of materials are air-stable<sup>12</sup> and have excellent mobility, the search for electron-transport materials that do not degrade when exposed to moisture or oxygen and perform comparably to best p-type materials continues.<sup>13</sup>

There are a few reports discussing n-type OFETs with increased air stability. They are typically based on novel derivatives of perylene diimides, naphthalene diimides, or quinones. Cyanated perylene diimidies have been found to have mobilities up to  $0.64 \ cm^2 V^{-1} s^{-1}$  with negligible degradation up to six months under ambient conditions. And the et al. have reported air stable PTCDI-C13 based OFETs with mobility of  $0.61 \ cm^2 V^{-1} s^{-1}$ . The mobility was maintained at 90% after 4 days and 59% after 105 days. Anthopolous et al. have reported [84]PCBM-based OFETs

with mobility of  $0.5 \times 10^{-3} \ cm^2 V^{-1} s^{-1}$  that remain stable for several months. <sup>16</sup> Mamada et al. have reported OFETs based on a quinone derivative <sup>17</sup> that retain a mobility of about  $0.1 \ cm^2 V^{-1} s^{-1}$  after one day. <sup>17</sup> The common theme is that these compounds tend to have low-lying lowest unoccupied molecular orbital (LUMO) levels, which enhance their stability. <sup>18</sup>

Overall, the performance of these n-type materials, although showing an improved stability, is not as good as the best p-type materials, which makes it difficult to design complimentary circuits, and to benefit from its low static power consumption.<sup>19</sup>

Fullerene  $C_{60}$  is one of the best-performing n-type organic semiconductors,<sup>20</sup> with mobilities reaching up to 5  $cm^2V^{-1}s^{-1}$ ,<sup>21</sup> but it is also known to degrade very quickly upon exposure to air, primarily due to oxygen and moisture. Oxygen and moisture are swiftly physiosorbed into the  $C_{60}$  lattice introducing deep trap states that capture electrons, resulting in a stark decrease in conductivity.<sup>22</sup> Oxygen essentially has a p-doping effect in  $C_{60}$  as observed by the shift in n-channel threshold voltage towards higher positive voltages.<sup>23</sup>

The success of  $C_{60}$ -based OFET devices has inspired the synthesis and testing of a large number of  $C_{60}$  derivatives. Of the 88 fullerene derivatives discussed in the review by Zhang et al.,<sup>20</sup> none of the fullerene derivatives that were tested had a mobility higher than  $0.5 \ cm^2 V^{-1} s^{-1}$  and only one fullerene derivative had a mobility higher than  $0.3 \ cm^2 V^{-1} s^{-1}$ . Additionally, none of the organic fullerene derivatives can be sublimed to make pristine solvent-free devices, which limits the device processing techniques that can be used. In some cases, such as PCBM, the fullerene derivative decomposes during the deposition process.<sup>24</sup> We recently reported the first example of the fullerene derivative-based n-type OFET devices fabricated via vapor deposition, with average electron mobility of  $0.34 \ cm^2 V^{-1} s^{-1}$ .<sup>25</sup> The electron transport material, 1.9- $C_{60}(cyclo$ - $CF_2(2$ - $C_{6}F_4)$ ), or  $C_{60}$  fauxhawk fullerene,  $C_{60}FHF$ , can be sublimed without decomposition, and at lower

temperature than the parent fullerene  $C_{60}$ . The thermal stability of fauxhawk has been attributed to the strong C–F bonds in the fauxhawk substituent vs the C–H bonds found in typical organofullerenes.

Based on this progress, we aim at developing high-performance, and air stable n-type semiconductors based on derivatized fullerenes. The following considerations must be taken into account to combine high performance and stability: i) a lower-lying LUMO is necessary to alleviate the likelihood of reaction between the electron carrier and water or oxygen; ii) the LUMO must align with the Fermi level of the electrode for efficient charge injection; iii) the adiabatic electron affinity should be large, i.e., 2.8 eV; $^{18,26}$  iv) thermal stability is desirable so that the material can be deposited via sublimation without degradation; v) the molecular structures of derivatized fullerenes should have a large number of  $\pi$ -bonds and allow for short inter-fullerene cage-to-cage distances to improve  $\pi$ - $\pi$  contact and mobility. Addition of functional groups to a fullerene disrupts the  $\pi$ -system, and larger substituents typically increase the inter-fullerene cage-to-cage distances, which can have an insulating effect. Thus, it is desirable to have a small number of substituents that have minimal steric bulk.

C<sub>60</sub>CF<sub>2</sub> (cf. Figure 1b) is a fullerene derivative that meets all of these requirements. Fluorine being the most electronegative atom is expected to increase the electron affinity of C<sub>60</sub>, which is desirable for n-type materials.<sup>26</sup> Indeed, recently, we have shown that C<sub>60</sub>CF<sub>2</sub> can be substituted for C<sub>60</sub> as the fullerene acceptor in organic photovoltaic (OPV) devices to achieve a power conversion efficiency (PCE) of 2.27 %.<sup>28</sup> C<sub>60</sub>CF<sub>2</sub> has a LUMO shift of 150 mV vs C<sub>60</sub><sup>29</sup> derived from Cyclic Voltammetry(CV) measurements. The gas phase electron affinity (EA<sub>g</sub>) was measured by low temperature photoelectron spectroscopy and found to be 2.88 eV, <sup>28</sup> right in the range of of 2.8-3.7 eV reported for materials demonstrating long-term stability. The lowest

unoccupied molecular orbital (LUMO) energy ( $E_{\rm LUMO}$ ) from DFT<sup>28</sup> calculations agrees reasonably with the LUMO shift derived from CV measurements. In bilayer OPV reference devices, in which an absorbing donor layer was absent, there was an even larger 330 mV shift in open circuit voltage ( $V_{\rm OC}$ ). This suggests that there is a larger difference in LUMO between C<sub>60</sub> and C<sub>60</sub>CF<sub>2</sub> in the solid state, which will be accounted for in OFET devices.

In this paper, the performance and stability of vacuum deposited  $C_{60}CF_2$  used as the electron transport material in bottom gate-top contact OFETs is explored. It is shown that  $C_{60}CF_2$ -based OFETs reach an average electron mobility of  $\mu = 0.83 \pm 0.52 \ cm^2 V^{-1} s^{-1}$ . Although the mobility is lower than the one of optimized  $C_{60}$  transistors ( $\mu = 2.26 \pm 0.81 \ cm^2 V^{-1} s^{-1}$ ) right after processing,  $C_{60}CF_2$  OFETs outperform  $C_{60}$  OFETs by an order of magnitude after prolonged exposure to ambient air. Overall, a mobility of  $\mu = 0.14 \pm 0.13 \ cm^2 V^{-1} s^{-1}$  is observed after 36h of exposure, and the shift of the threshold voltage is limited to approx. 1V.

## **EXPERIMENTAL DETAILS**

The synthesis of C<sub>60</sub>CF<sub>2</sub> is described in the supplemental information. A schematic structure of the devices used in the experiment is shown in **Figure 1a**. The devices are prepared on glass substrates. The substrate is cleaned by sonicating in DI water for 20 mins at 60°C followed by rinsing with DI water, acetone, methanol and isopropanol successively before blow drying it. Following cleaning, a gate comprising of a 150 nm layer of aluminum is deposited in a vacuum chamber (Angstrom Engineering, EvoVac) by thermal evaporation.

Following aluminum deposition, the samples are subject to electrochemical anodization to grow a layer of aluminum oxide. A 1 mM aqueous solution of citric acid is used as the electrolyte. The substrates are immersed in the electrolyte such that the gate areas are fully immersed. A constant

current bias of  $I = 0.1 \, mA$  is supplied to the substrate at the anode.<sup>30</sup> A reference platinum electrode is used as cathode. As the oxide grows the potential between the anode and the cathode increases until it reaches a set maximum value (the anodization voltage  $V_{Anode}$ ). Once this value is reached, the potential is kept constant and the anodization current decays exponentially as the oxide continues to grow. The process is stopped once the current reaches about 10% of its initial value, which takes about 750 s. The thickness of the oxide is controlled solely by the anodization voltage  $V_{Anode}$  and a growth rate of around 1.3 nm/V for the anodization conditions used in our experiment were reported.<sup>30</sup> At an anodization voltage of  $V_{Anode} = 24 \, V$  as used here, we obtain an oxide layer with a thickness of  $d_{ox} \cong 30 \, nm$ .

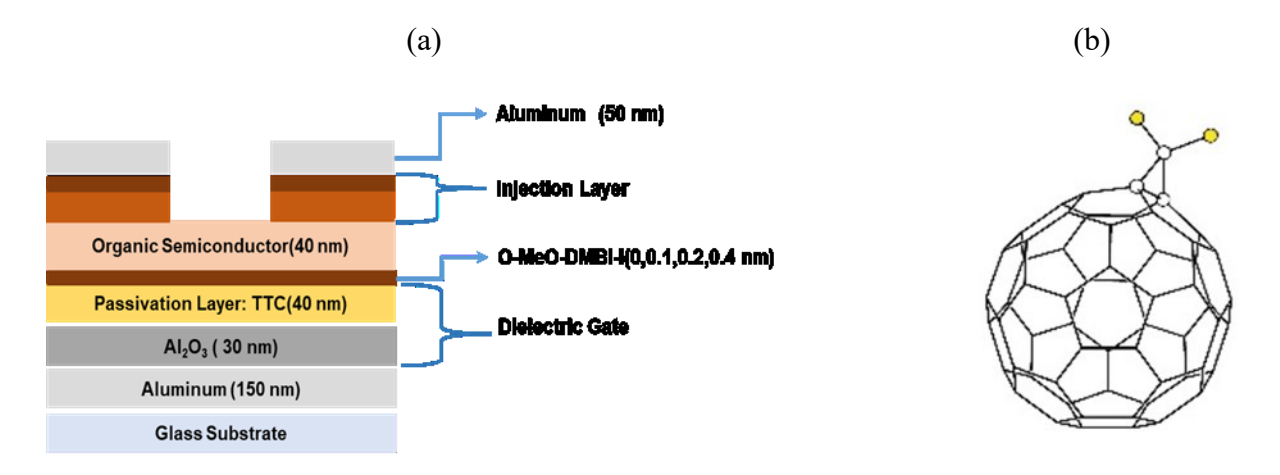


Figure 1: (a) Schematic structure of the OFETs used in our experiment (b) Structure of the C60CF2 molecule

Following anodization, the substrates are loaded in the vacuum chamber and a 40 nm thick passivation layer of tetratetracontane (TTC) is deposited with the substrate held at a temperature of T = 55°C. Following the deposition, the samples are annealed in the vacuum chamber for 1 h at T = 55°C. These conditions were found to give the best performance in terms of mobility and hysteresis. The organic semiconductor ( $C_{60}CF_2$ , cf. **Figure 1b**, or  $C_{60}$ ) layer is then deposited,

followed by the source and drain contacts. Two different types of injection layers are tested: gold and a n-type injection layer consisting of a stack of a 25 nm layer of C<sub>60</sub> doped with O-MeO-DMBI-I (4 and 8 wt.%) and a 2nm layer of pure dopant. Aluminum is deposited on top of the injection material to improve lateral conduction of the source and drain contact.

A total of 16 samples arranged in a 4x4 array were processed. Of these, 3 rows (one row with 4 samples for each source/drain contact) have  $C_{60}CF_2$  as the organic semiconductor and one row is processed with  $C_{60}$  for comparison. Along the columns of the array, the transistor channel was doped by a thin pure layer of o-MeO-DMBI-I, which is known to provide a well-controlled doping effect without significantly disturbing the charge carrier mobility in the films.<sup>25</sup> The thickness of the dopant layer was varied from  $d_{dop} = 0, 0.1, 0.2, 0.4 \, nm$ , yielding all combinations of dopant layer thickness and type of injection layer.

Each sample consists of 12 transistors with 6 different channel lengths (100, 150, 200, 250, 300 and 350  $\mu$ m). Of the 192 transistors processed (16 samples, 12 transistors each), 162 are working and are included in the analysis. Samples were excluded if they showed no current modulation as expected from a transistor or if there was a large gate leakage.

C<sub>60</sub> is obtained from Sigma Aldrich with a purity of 99.9%. All is supplied by Kurt J. Lesker with a purity of 99.99%. TTC is obtained from Sigma Aldrich with a purity of 99%. Gold is obtained from Angstrom Engineering with a purity of 99.99%. All layers are deposited by thermal evaporation with a base pressure of 10<sup>-7</sup> Torr and structured by shadow masks. All electrical characterization is done in a nitrogen filled glovebox using a Keithley 4200 parameter analyzer. The evaporation chamber and glovebox are manufactured by Angstrom Engineering.

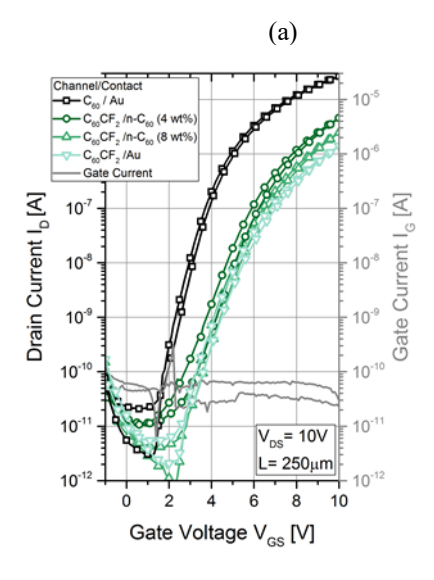
#### **RESULTS**

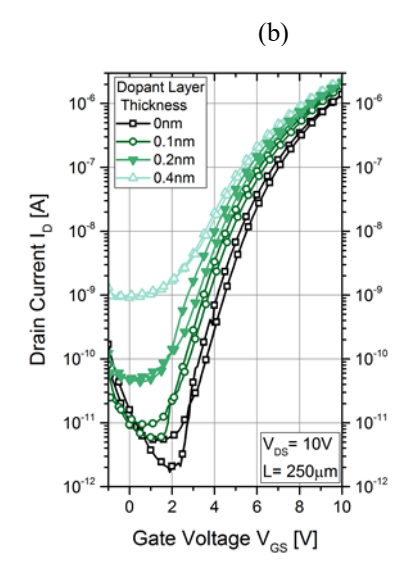
The transfer characteristics of representative  $C_{60}CF_2$  OFETs with different injection layers (Au,  $C_{60}$ : 4wt.%O-MeO-DMBI-I and  $C_{60}$ : 8wt.%O-MeO-DMBI-I) are plotted in **Figure 2a**. The transfer characteristic of a  $C_{60}$  OFET with gold injection layer prepared in the same run, i.e. under identical process conditions, is also plotted for comparison. The gate current is well controlled ( $I_G \sim 100 \ pA$ ) in all samples. Overall, the samples reach an ON/OFF ratio of approx. 6 ( $C_{60}$ ) or 5 ( $C_{60}CF_2$ ) orders of magnitude.

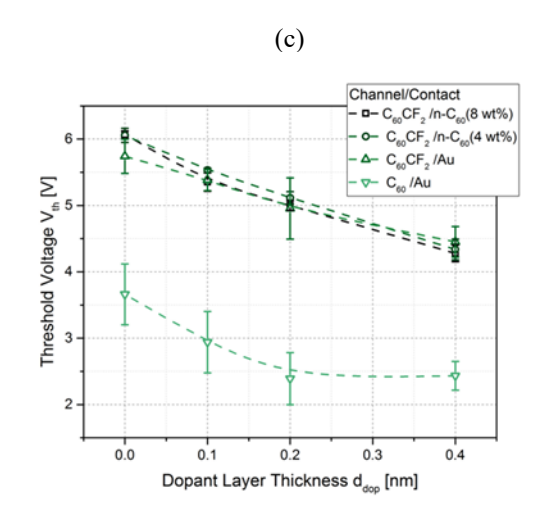
Without exposure to ambient air,  $C_{60}$  samples show a better performance than  $C_{60}CF_2$ , i.e. the on current at  $V_{GS}=10~V$  is about one order of magnitude larger for  $C_{60}$ . This increased current correlates with a higher electron mobility. The average mobility of  $C_{60}$  OFETs with gold contacts without channel doping is  $\mu=(2.26~\pm~0.81)cm^2V^{-1}s^{-1}$ . The average mobility for  $C_{60}CF_2$  OFETs with gold contacts and no dopant layer is  $\mu=(0.83~\pm~0.52)cm^2V^{-1}s^{-1}$ .

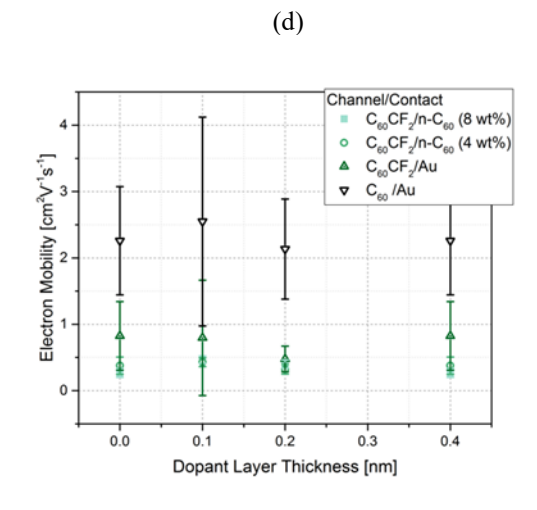
The transfer characteristics of  $C_{60}CF_2$  OFETs with gold contacts having different thickness of dopant layer are plotted in **Figure 2b.** There is a clear shift in threshold voltage  $V_{th}$  and increase in off-current with increasing thickness of dopant layer. At dopant layer thickness of 0.4 nm the off current is in the range of 1 nA, i.e. significantly increased compared to the intrinsic case. The detailed statistics of threshold voltage and mobility are discussed in **Figure 2c** and **Figure 2d**, respectively. The threshold voltage for undoped  $C_{60}$  OFETs is  $V_{th} = (3.66 \pm 0.64) V$ , while the average threshold voltage for  $C_{60}CF_2$  OFETs without dopant layer range from  $V_{th} = (5.74 \pm 0.26)V$  for gold contacts to  $V_{th} = (6.05 \pm 0.11) V$  and  $V_{th} = (6.07 \pm 0.05) V$  for doped n-type contacts with 4wt.% and 8wt.% doping, respectively.

The trends of the shift in threshold voltage shown in **Figure 2c as well** can be explained by a simple analytical model proposed previously for OFETs doped by a thin bulk layer of dopant at the gate dielectric/organic









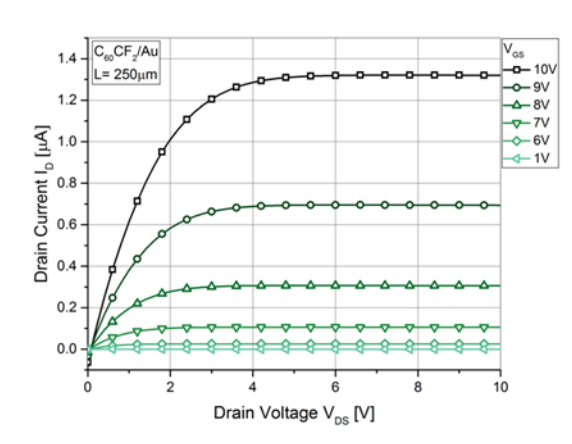


**Figure 2:** (a) Transfer Characteristics of C<sub>60</sub>CF<sub>2</sub> OFETs with different injection layers and C<sub>60</sub> OFET with gold injection layer (b) Transfer characteristics of C<sub>60</sub>CF<sub>2</sub> OFETs with gold injection layer and varying thickness of dopant layer (c) Threshold voltage statistics of C<sub>60</sub> and C<sub>60</sub>CF<sub>2</sub> OFETs (d) Mobility statistics of C<sub>60</sub> and C<sub>60</sub>CF<sub>2</sub> OFETs (e) Output characteristic of C<sub>60</sub>CF<sub>2</sub> OFET with gold injection layer.

semiconductor interface.<sup>25,31</sup> Assuming that the bulk dopant layer introduces a density of  $N_D^{\bullet}$  free electrons per unit area in the channel, one obtains for the threshold voltage  $V_{th}$ 

$$V_{th} = V_{FB} - \frac{eN_D^{\bullet}}{c_i}, \tag{Eq. 1}$$

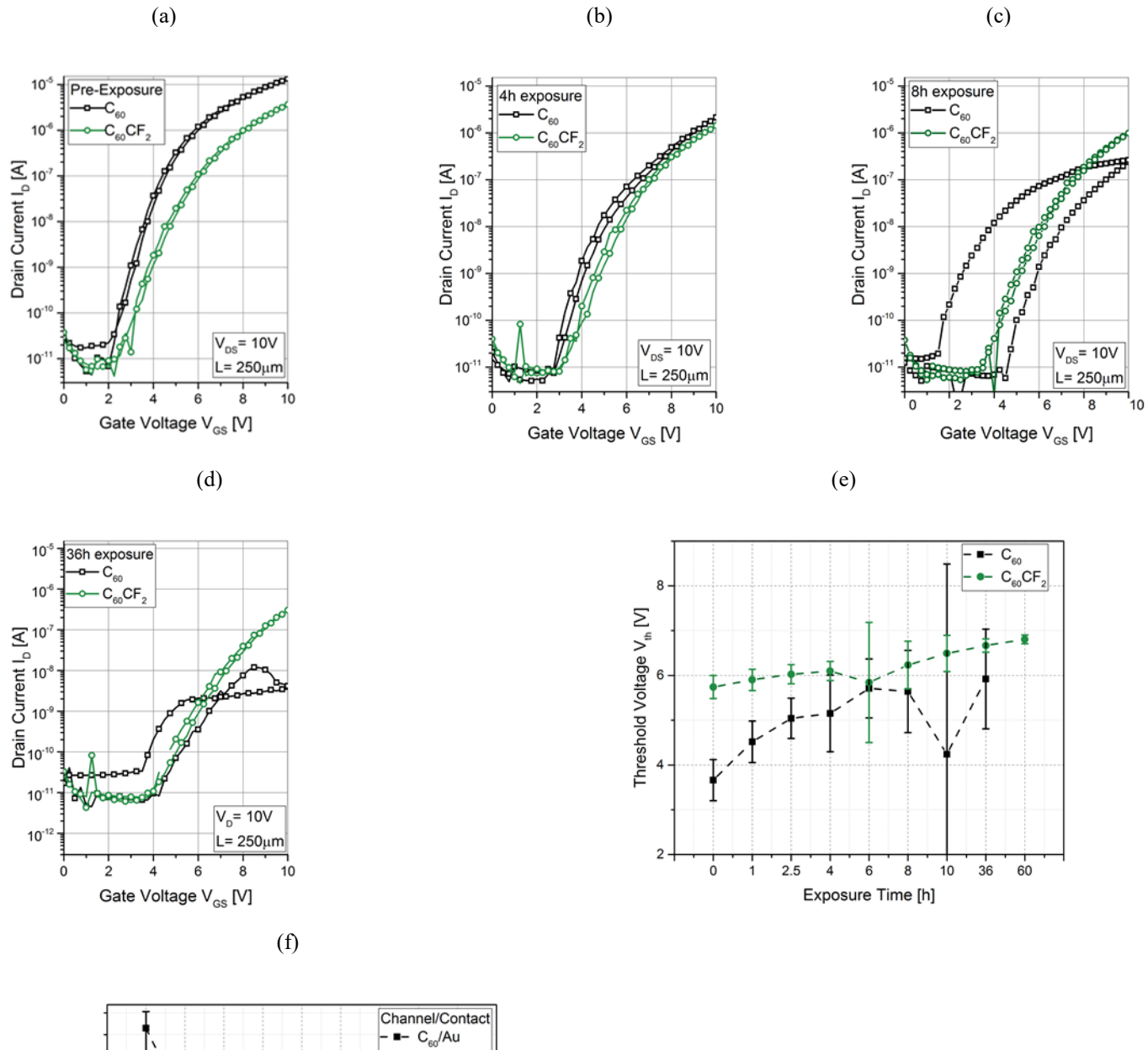
where  $V_{FB}$  is the flatband voltage of the gate capacitor, e is the elementary charge, and  $C_i$  is the capacitance per unit area of the gate. Following Eq. 1, the shift in threshold voltage observed for increasing thickness of the dopant layer can be explained by an increase in  $N_D^{\blacksquare}$ . One can estimate that doping introduces between  $1.1 \times 10^{15} \,\mathrm{m}^{-2} (d_{dop} = 0.1 \,nm)$  and  $3.6 \times 10^{15} \,\mathrm{m}^{-2} (d_{dop} = 0.4 \,nm)$  free charges inside the transistor channel.

Figure 2c shows as well that there is an almost constant difference in threshold voltage  $V_{th}$  of approx. 2V between  $C_{60}$  and  $C_{60}CF_{2}$ , independent of the dopant layer thickness  $d_{dop}$ . Considering Eq. 1, this difference could be explained by a shift in the flatband voltage  $V_{FB}$ . Assuming an ohmic contact at the source electrode, the flatband voltage is defined by

$$V_{FB} = \frac{1}{e} \left( W_f - (EA + \eta) - \delta - \frac{Q_{trap}}{C_i} \right), \quad (Eq. 2)$$

where  $W_f$  is the work-function of the gate metal, EA is the electron affinity of the organic semiconductor (or LUMO),  $\eta$  is the energetic distance of the Fermi Level inside the organic semiconductor and EA,  $\delta$  are interface dipoles either at the source/organic semiconductor interface or at the gate dielectric/organic semiconductor interface, and  $Q_{trap}$  are interface or bulk traps. Except for the work-function of the gate electrode, which is identical for  $C_{60}$  and  $C_{60}CF_2$  transistors, all parameters of Eq. 2 can contribute to the shift in threshold voltage. For example, the CV-derived shift in LUMO  $\Delta$ EA due to functionalization of  $C_{60}$  by  $CF_2$  is about 150 meV<sup>28</sup>, which can reach 330 meV in solid state. Similarly, a difference in the Fermi Level level in the bulk  $\eta$ , or a different density of bulk traps are possible reasons for the offset in threshold voltage.

The average mobility of the devices for different dopant layer thickness is discussed in **Figure 2d.** In general, the C<sub>60</sub> devices have a higher mobility compared to the C<sub>60</sub>CF<sub>2</sub> devices. Among the C<sub>60</sub>CF<sub>2</sub> devices, the ones with gold injection layer show the best mobility. The average mobility of C<sub>60</sub> OFETs with gold contacts and without dopant layer is  $\mu = (2.26 \pm 0.81)cm^2V^{-1}s^{-1}$ . The average mobility for C<sub>60</sub>CF<sub>2</sub> OFETs with gold contacts and without dopant layer is  $\mu = (0.83 \pm 0.52) cm^2V^{-1}s^{-1}$ , which is still amongst the best performance for functionalized fullerenes.<sup>13</sup> Some devices even have mobility as high as  $\mu = 2.02 cm^2V^{-1}s^{-1}$ , however this result has to be seen as a statistical outlier. Similar C<sub>60</sub>CF<sub>2</sub> OFETs with doped n-type injection layer have average mobilities of  $\mu = (0.38 \pm 0.13) cm^2V^{-1}s^{-1}$  and  $\mu = (0.27 \pm 0.06) cm^2V^{-1}s^{-1}$  for doped n-type contacts with doping concentrations of 4wt.% and 8wt.% respectively. Therefore, based on



U.01 0 1 2.5 4 6 8 10 36 60

Exposure Time [h]

**Figure 3:** (a) Transfer Characteristics of a  $C_{60}CF_2$  and  $C_{60}$  OFET with gold injection layer before exposure to air (b) after 4 h (c) ) after 8 h and (d) after 36 h of exposure (e) Average threshold voltage of  $C_{60}$  and  $C_{60}CF_2$  OFETs versus exposure time (f) Average mobility of  $C_{60}$  and  $C_{60}CF_2$  OFETs versus exposure time.

the threshold voltage and mobility data it appears that gold is best suited for optimal performance in C<sub>60</sub>CF<sub>2</sub> OFETs. Matching the work function of the injection contact to the HOMO/LUMO of the OSC is considered an excellent guide for contact selection leading to optimal performance. However, it is routinely observed in our experiments with fullerene and pentacene OFETs including this one that gold contacts provide better injection than doped contacts despite a larger energy level mismatch. While matching the energy levels at the interface is a reasonable rule of thumb for contact selection, the actual picture is more complex.

To study the relative air-stability of C<sub>60</sub> and C<sub>60</sub>CF<sub>2</sub> OFETs, only devices with gold injection layer and without dopant layer are chosen to focus on effects that occur due to the organic semiconductor layer or at the OSC/dielectric interface. The exposure was done under ambient light and humidity conditions (approx. 40% relative humidity). One substrate of each kind (consisting of 12 OFETs each) is removed from the glovebox and exposed to ambient air for a specific amount of time, after which it is returned and electrically characterized in the glovebox. This process is repeated for a total of up to 60 h of exposure.

The transfer characteristics of a representative  $C_{60}$  and  $C_{60}CF_2$  OFET before exposure is plotted in **Figure 3a**, showing that in accordance with **Figure 2c** and **d** the  $C_{60}$  OFET has a smaller threshold voltage and larger mobility initially. Upon exposure to air the OFETs are expected to degrade. The threshold voltage is expected to increase, and the mobility is expected to decrease. After 4 h of exposure it can be seen that the  $C_{60}$  and  $C_{60}CF_2$  OFET have similar performance, i.e. the  $C_{60}$  OFET degrades at a faster rate (**Figure 3b**). After 8 h, the  $C_{60}$  OFETs acquire a large hysteresis and show significant degradation in terms of mobility and threshold voltage, whereas the  $C_{60}CF_2$  OFETs still show no hysteresis and a relatively small change in threshold voltage and mobility (**Figure 3c**). Finally, after 36 h of exposure, the  $C_{60}$  OFETs have almost completely

degraded and only few of them show any current modulation, as seen in **Figure 3d**. The C<sub>60</sub>CF<sub>2</sub> OFETs still function, albeit with a lower mobility and larger threshold.

The average threshold voltage and mobility for the  $C_{60}$  and  $C_{60}CF_2$  samples with exposure time are plotted in **Figure 3e** and **Figure 3f**, respectively. It is clear that the  $C_{60}$  OFETs degrade at a faster rate as seen by the steeper rise in threshold voltage and steeper fall in mobility. After 36 h of exposure,  $C_{60}$  OFETs show an increase in average threshold voltage from  $V_{th} = 3.66 \pm 0.46 \, V$  to  $V_{th} = 5.92 \pm 1.11 \, V$  and mobility drop from  $\mu = 2.26 \pm 0.81 \, cm^2 V^{-1} s^{-1}$  to  $\mu = 0.016 \pm 0.013 \, cm^2 V^{-1} s^{-1}$ . For  $C_{60}CF_2$  OFETs, the decrease in performance is much smaller. The threshold voltage only increases from  $V_{th} = 5.74 \pm 0.26 \, V$  to  $V_{th} = 6.67 \pm 0.15 \, V$  and the mobility drops from  $\mu = 0.83 \pm 0.52 \, cm^2 V^{-1} s^{-1}$  to  $\mu = 0.14 \pm 0.13 \, cm^2 V^{-1} s^{-1}$ .

A few mechanisms for the degradation of channel mobility are discussed in literature and it was reported that both oxygen and moisture play and important role in the degradation of OFETs.<sup>33</sup> For example, it has been shown that water leads to degradation of Pentacene OFETs by the introduction of mobile species into the film.<sup>34</sup> Furthermore, Hwang et al. showed that for n-type polymer OFETs based on P(NDI2OD-T2), both oxygen and water form traps.<sup>35</sup> Additionally, it has been suggested that hydrated oxygen complexes such as H<sub>2</sub>O-O<sub>2</sub> and (H<sub>2</sub>O)<sub>2</sub>-O<sub>2</sub> contribute to deep trap sites.<sup>36,37</sup> To clarify the relative contribution of oxygen and moisture to the degradation observed here, the OFETs were annealed at 60°C for 1h in a nitrogen filled glovebox (oxygen content in the 1 ppm regime). Degradation due to exposure to pure oxygen was shown to be partially reversible by annealing the films in vacuum. Although some improvement in mobility was found, the increase was small and within the standard deviation of the spread in mobility. This indicates that the observed mechanism is not merely due to a p-doping effect of oxygen in the

fullerene film, but that the films are permanently damaged, most likely caused by new trap states caused by hydrated complexes as e.g. proposed by Zhuo et al. <sup>36</sup>.

Overall, **Figure 3** confirms our hypothesis of enhanced air-stability. The addition of the -CF<sub>2</sub> side group to the fullerene leads to a smaller shift in threshold voltage and degradation of mobility during exposure to ambient air. Although the material proposed here has a lower average mobility of 0.83 cm<sup>2</sup>V<sup>-1</sup>s<sup>-1</sup> compared to C<sub>60</sub> transistors, this performance is still high compared to other fullerene derivatives and could be further improved by an optimization of the injection layer and deposition parameters.

#### **CONCLUSION**

A number of applications targeted by the OFET community require complementary circuits,

however, current n-type organic semiconductors lag behind p-type organic semiconductors in terms of their mobility and stability in ambient conditions. Most importantly, electron transport materials are inherently more susceptible to oxygen and moisture in the atmosphere, leading to a strong shift in threshold voltage and degradation in charge mobility when exposed to ambient air. Here, it is shown that functionalizing the electron conducting group of n-type organic semiconductors with fluorinated side groups leads to an increase in the stability of OFETs. A comparison between  $C_{60}$  and  $C_{60}CF_2$  OFETs indicate that  $C_{60}CF_2$  OFETs degrade at a much slower rate and sustain an exposure of up to 60h in ambient air. Although  $C_{60}CF_2$  shows a slightly lower performance compared to  $C_{60}$ ,  $C_{60}CF_2$  OFETs still reach an average mobility of  $\mu = 0.83 \pm 0.52 \ cm^2 V^{-1} s^{-1}$ , which is among the best performing n-type semiconductor materials with increased air stability.<sup>20,13</sup> The best performance is reached when using gold injection layers, but further optimization of contact materials and deposition conditions could increase the transistor performance further.

## **ACKNOWLEDGMENTS**

We thank the National Science Foundation (grant no. ECCS #1709479 and partially, grant no CHE# 362302) for funding this research. Characterization of samples was partially done at the Characterization Facility of the Advanced Materials and Liquid Crystal Institute of Kent State University.

# **SUPPORTING INFORMATION:**

- 1) Reagents and Materials
- 2) Synthesis of C60CF<sub>2</sub>
- 3) <sup>19</sup>F NMR spectrum and HPLC chromatogram of C<sub>60</sub>CF<sub>2</sub> sample

## REFERENCES

- 1. Zhou, L. *et al.* All-organic active matrix flexible display All-organic active matrix flexible display. *Appl. Phys. Lett.* **88**, 1–4 (2009).
- 2. Xiang, L., Wang, W. & Xie, W. Achieving high mobility, low-voltage operating organic

- field-effect transistor nonvolatile memory by an ultraviolet-ozone treating ferroelectric terpolymer. *Sci. Rep.* **6**, 1–10 (2016).
- 3. Sagdullina, D., Lukashkin, N., Parfenov, A., Lyssenko, K. & Troshin, P. Highly sensitive OFET-based gas sensors using fluorinated naphthalenediimide semiconductor films. *Synth. Met.* **260**, (2020).
- 4. Yamashita, Y. Organic semiconductors for organic field-effect transistors. *Sci. Technol. Adv. Mater.* **10**, (2009).
- 5. Lai, S. *et al.* A plastic electronic circuit based on low voltage, organic thin-film transistors for monitoring the X-Ray checking history of luggage in airports. *Org. Electron.* **58**, 263–269 (2018).
- 6. Klauk, H. Will We See Gigahertz Organic Transistors? *Adv. Electron. Mater.* **4**, 1–8 (2018).
- 7. Ahmed, R. *et al.* Reproducibility and stability of C 60 based organic field effect transistor. *Synth. Met.* **161**, 2562–2565 (2012).
- 8. Wang, C. Y. *et al.* Stable low-voltage operation top-gate organic field-effect transistors on cellulose nanocrystal substrates. *ACS Appl. Mater. Interfaces* **7**, 4804–4808 (2015).
- 9. Xiang, L., Wang, W. & Gao, F. Improving Mobility and Stability of Organic Field-Effect Transistors by Employing a Tetratetracontane Modifying PMMA Dielectric. *IEEE Trans. Electron Devices* **6**, 4440–4444 (2016).
- 10. Minemawari, H. et al. Inkjet printing of single-crystal films. *Nature* 475, 364–367 (2011).
- 11. Borchert, J. W. et al. Small contact resistance and high-frequency operation of flexible low-

- voltage inverted coplanar organic transistors. *Nat. Commun.* **10**, 1–11 (2019).
- 12. Zschieschang, U. *et al.* Flexible low-voltage organic thin-film transistors and circuits based on C 10-DNTT. *J. Mater. Chem.* **22**, 4273–4277 (2012).
- 13. Quinn, J. T. E., Zhu, J., Li, X., Wang, J. & Li, Y. Recent progress in the development of n-type organic semiconductors for organic field effect transistors. *J. Mater. Chem. C* **5**, 8654–8681 (2017).
- 14. Jones, B. A. *et al.* High-mobility air-stable n-type semiconductors with processing versatility: Dicyanoperylene-3,4:9,10-bis(dicarboximides). *Angew. Chemie Int. Ed.* **43**, 6363–6366 (2004).
- 15. Roh, J., Lee, J., Kang, C. M., Lee, C. & Jun Jung, B. Air stability of PTCDI-C13-based n-OFETs on polymer interfacial layers. *Phys. Status Solidi Rapid Res. Lett.* **7**, 469–472 (2013).
- 16. Anthopoulos, T. D. *et al.* Air-stable n-channel organic transistors based on a soluble C84 fullerene derivative. *Adv. Mater.* **18**, 1679–1684 (2006).
- 17. Mamada, M., Kumaki, D., Nishida, J. I., Tokito, S. & Yamashita, Y. Novel semiconducting quinone for air-stable n-type organic field-effect transistors. *ACS Appl. Mater. Interfaces* 2, 1303–1307 (2010).
- 18. Chang, Y. C., Kuo, M. Y., Chen, C. P., Lu, H. F. & Chao, I. On the air stability of n -channel organic field-effect transistors: A theoretical study of adiabatic electron affinities of organic semiconductors. *J. Phys. Chem. C* **114**, 11595–11601 (2010).
- 19. Zaumseil, J. & Sirringhaus, H. Electron and ambipolar transport in organic field-effect

- transistors. Chem. Rev. 107, 1296–1323 (2007).
- Zhang, Y., Murtaza, I. & Meng, H. Development of fullerenes and their derivatives as semiconductors in field-effect transistors: Exploring the molecular design. *J. Mater. Chem. C* 6, 3514–3537 (2018).
- 21. Li, H. *et al.* High-mobility field-effect transistors from large-area solution grown aligned C\_{60} single crystals. *J. Am. Chem. Soc.* **134**, 2760–2765 (2012).
- 22. Ahmed, R., Simbrunner, C., Schwabegger, G., Baig, M. A. & Sitter, H. Air stability of C60 based n-type OFETs. *Synth. Met.* **188**, 136–139 (2014).
- 23. Qiu, Y. *et al.* Manipulating Doping of Organic Semiconductors by Reactive Oxygen for Field-Effect Transistors. *Phys. Status Solidi Rapid Res. Lett.* **12**, 1–8 (2018).
- 24. Larson, B. W. *et al.* Thermal  $[6,6] \rightarrow [6,6]$  isomerization and decomposition of PCBM (phenyl-C61-butyric acid methyl ester). *Chem. Mater.* **26**, 2361–2367 (2014).
- 25. Liu, S. *et al.* Doped N-Type Organic Field-Effect Transistors Based on Faux-Hawk Fullerene. *Adv. Electron. Mater.* **5**, 1–9 (2019).
- 26. Tokunaga, K., Ohmori, S. & Kawabata, H. Theoretical study on possible usage of difluoromethylene fullerenes as electron-transport materials. *Thin Solid Films* **518**, 477–480 (2009).
- Zhang, Y., Murtaza, I. & Meng, H. Development of fullerenes and their derivatives as semiconductors in field-effect transistors: Exploring the molecular design. *J. Mater. Chem. C* 6, 3514–3537 (2018).

- 28. Reeves, B. J. *et al.* Fluorous Fullerene Acceptors in Vacuum-Deposited Photovoltaic Cells. *Sol. RRL* **3**, 1900070 (2019).
- 29. Boltalina, O. V., Popov, A. A., Kuvychko, I. V., Shustova, N. B. & Strauss, S. H. Perfluoroalkylfullerenes. *Chem. Rev.* **115**, 1051–1105 (2015).
- 30. Dang, X. D., Plieth, W., Richter, S., Plötner, M. & Fischer, W. J. Aluminum oxide film as gate dielectric for organic FETs: Anodization and characterization. *Phys. Status Solidi Appl. Mater. Sci.* **205**, 626–632 (2008).
- 31. Lüssem, B. *et al.* Doped organic transistors operating in the inversion and depletion regime.

  Nat. Commun. 4, 1–6 (2013).
- 32. Tietze, M. L., Burtone, L., Riede, M., Lüssem, B. & Leo, K. Fermi level shift and doping efficiency in p-doped small molecule organic semiconductors: A photoelectron spectroscopy and theoretical study. *Phys. Rev. B Condens. Matter Mater. Phys.* **86**, (2012).
- 33. Zschieschang, U. *et al.* Separating the impact of oxygen and water on the long-term stability of n-channel perylene diimide thin-film transistors. *Org. Electron.* **26**, 340–344 (2015).
- 34. Li, D. *et al.* Humidity effect on electrical performance of organic thin-film transistors. *Appl. Phys. Lett.* **86**, 2003–2006 (2005).
- 35. Hwang, D. K. *et al.* Systematic reliability study of top-gate p- and n-channel organic field-effect transistors. *ACS Appl. Mater. Interfaces* **6**, 3378–3386 (2014).
- 36. Zhuo, J. M. *et al.* Direct spectroscopic evidence for a photodoping mechanism in polythiophene and poly(bithiophene-alt-thienothiophene) organic semiconductor thin films involving oxygen and sorbed moisture. *Adv. Mater.* **21**, 4747–4752 (2009).

37. Nicolai, H. T. *et al.* Unification of trap-limited electron transport in semiconducting polymers. *Nat. Mater.* **11**, 882–887 (2012).